Supplementary Information (SI) for New Journal of Chemistry.
This journal is © The Royal Society of Chemistry and the Centre National de la Recherche Scientifique 2024

Ag@Ca-MOF Composite: A Dual-Function Material for Luminescent Detection and Dose Reliant Photocatalytic Breakdown of Bisphenol A

Vibhav Shukla[a], Gulshitab Aalam[b], S. Wazed Ali[b,c], Musheer Ahamd[d], Nazrul Haq[e], Kafeel Ahmad Siddiqui[a]

[a]Department of Chemistry, National Institute of Technology Raipur, G E Road Raipur – 492010, Chhattisgarh, India

[b]School of Interdisciplinary Research (SIRe), Indian Institute of Technology Delhi, Hauz Khas, New Delhi, 110016, India

[c]Department of Textile and Fibre Engineering, Indian Institute of Technology Delhi, Hauz Khas, New Delhi, 110016, India

[d]Department of Applied Chemistry, Faculty of Engineering and Technology, ZHCET, Aligarh Muslim University, Aligarh, UP (India) – 202002

[e]Department of Pharmaceutics, College of Pharmacy, King Saud University, Riyadh 11451, Saudi Arabia

[a] Corresponding Author: Dr. Kafeel Ahmad Siddiqui[a] e-mail: kasiddiqui.chy@nitrr.ac.in

S 1. Photocatalyst Degradation of BPA with Ca-MOF

S 1.1 Photocatalytic Activity of Bisphenol A

Bisphenol A (BPA) is utilized to investigate the photocatalytic characteristics of the freshly prepared pure sample $\{[Ca(Cei)(H_2O)_2].3H_2O\}_n$ (**Ca-MOF)**. When exposed to visible sun light, BPA break down. The size, shape, component concentration, and crystal structure of the catalyst are important factors that have a substantial impact on the photocatalyst's activity. The efficiency of photocatalytic degradation was assessed by monitoring changes in the distinct UV-Vis absorption spectra of model BPA contaminants, which were exposed to sunlight and

subsequently faded. The UV-Vis absorption spectra of the BPA solution treated with **Ca-MOF** under sun radiation are shown in a time-dependent Fig. S1.

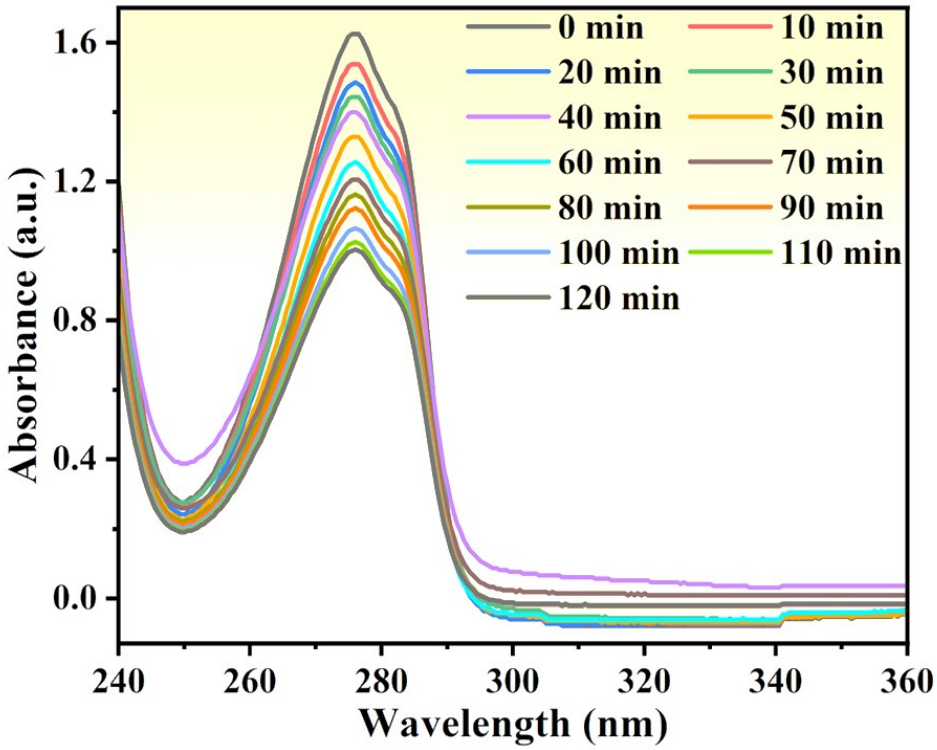

Fig. S1. UV-Vis absorption spectra of BPA solution containing **Ca-MOF** under 120 min time-dependent sunlight irradiation.

The degradation efficiency was determined utilizing the equation (1):

$$Degradation\ \% = \{(C_0 - C_t)/C_0\} \times 100 \quad (1)$$

C_0 represents the initial concentration and C_t shows the concentration at time t of the aqueous BPA solution.

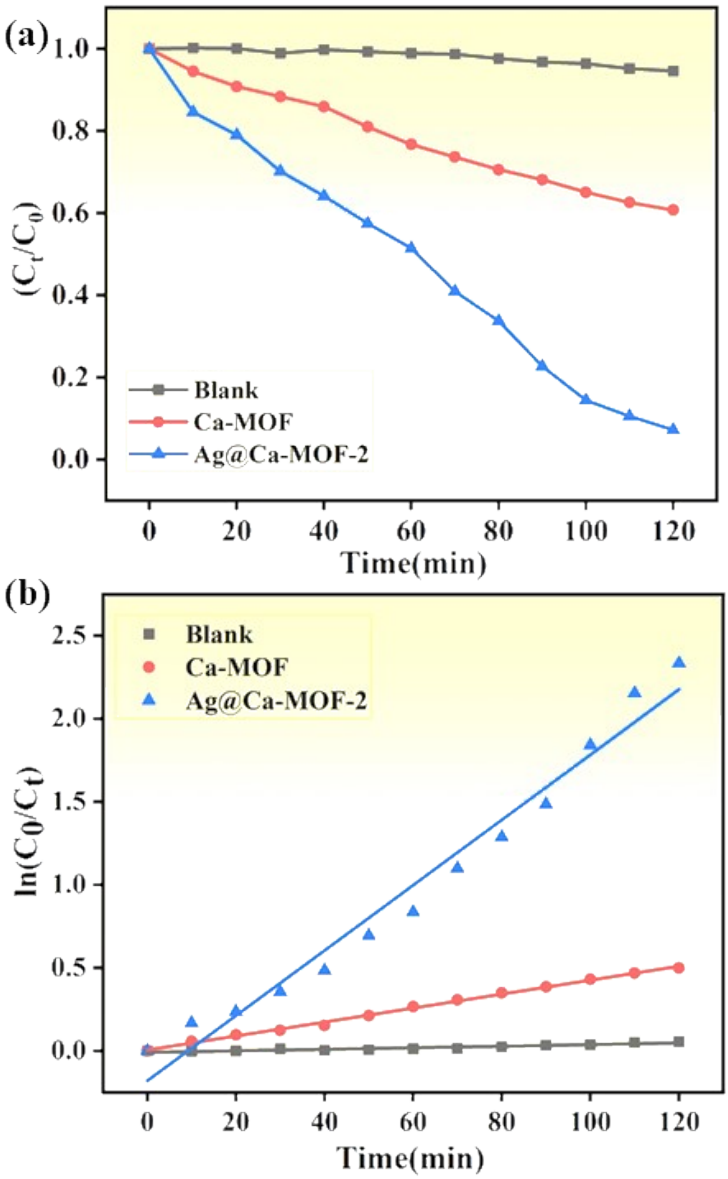

Fig. S2. Photocatalytic degradation kinetic plot: (a) Plot of C_0/C_t versus time interval (b) Plot of $\ln(C_0/C_t)$ versus time interval by **Ca-MOF** under 120 minutes of visible sunlight irradiation.

$\{[Ca(Cei)(H_2O)_2].3H_2O\}_n$ (**Ca-MOF)** achieved a degrading efficiency of about 37.52% for BPA after being exposed to visible light for 120 minutes (Fig. S1). The photocatalytic degradation kinetic plot of $\ln(C_0/C_t)$ versus time interval and C_t/C_0 vs time interval, respectively, is displayed in Fig. S2a and S2b. When analyzing the breakdown of BPA in aqueous solution,

the pseudo-first-order kinetic rate equation is frequently used. Equation (2) can be used to define the pseudo-first order kinetic model.

$$\ln(C_0/C_t) = k\,t \quad (2)$$

C_0 and C_t represent the starting concentration and concentration at time t of an aqueous BPA solution, respectively. The variable k denotes the first-order rate constant of the reaction. A linear relationship may be observed by graphing the natural logarithm of the ratio of the initial concentration (C_0) to the concentration at a given time (C_t) over time. The slope of this line corresponds to the value of the first-order rate constant (k). The rate constant value for BPA is 0.00415 min^{-1}. Equation (3) can be utilized to determine the half-life time ($t_{1/2}$) of the reaction:

$$t_{1/2} = ln2/k \quad (3)$$

Under the same photocatalytic conditions, it is evident that BPA degrades at a lower rate for Ca-MOF-2 as compared to Ag@Ca-MOF-2 composite utilized in the reaction process. This is due to the much higher half-life of the BPA degradation reaction (166.77 min). \

S 1.2 Analyzing of Reusability and Stability

After all associated BPA had totally degraded, the $\{[Ca(Cei)(H_2O)_2].3H_2O\}_n$ (**Ca-MOF)** capacity for recycling was examined. The **Ca-MOF** was extracted through filtration, repeatedly cleaned, dried, and then used one more. Five iterations of this were conducted, and Fig. S3 displays the **Ca-MOF** reusability outcome for each cycle in terms of degrading efficiency (%). Findings showed that during the course of the five cycles, there was a decrease in declining efficiency. Despite the decline in efficiency, powder X-ray diffraction (PXRD) analysis was conducted after five cycles to evaluate the catalyst's structural integrity. The PXRD pattern, as depicted in Fig. S21, confirms that the molecular framework of Ca-MOF remained stable, with no significant structural changes detected after repeated use.

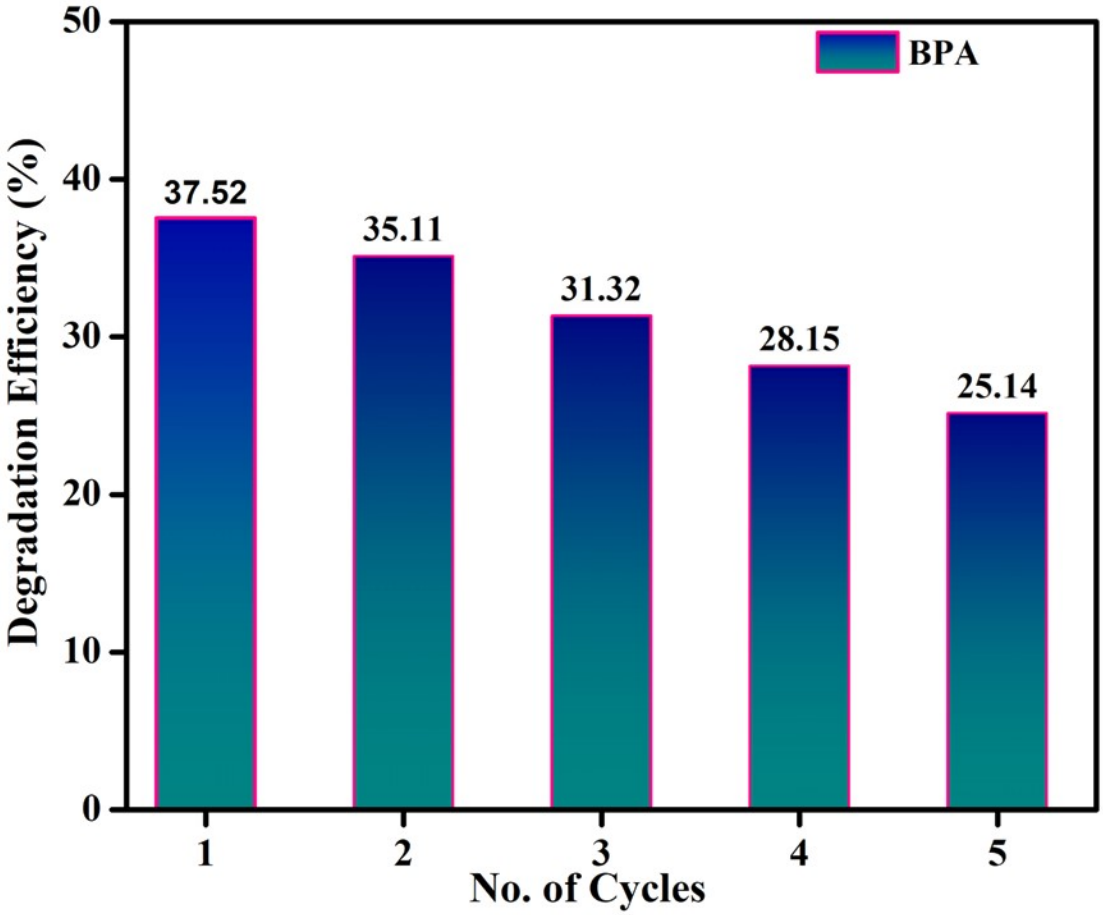

Fig. S3 Degradation efficiency of Ca-MOF for BPA over five cycle.

S 1.3 Determining Influence: The Impact of Initial pH Values

The pH level of the solution is a pivotal factor influencing the efficacy of the catalytic degradation process. Employing this methodology has yielded the development of exceptionally stable Coordination Polymers, demonstrating remarkable durability against water and a diverse range of pH conditions for a duration of no less than 24 hours (covering the pH range from 0 to 12). In investigating the influence of pH on the efficacy of photocatalytic degradation of BPA, the pH of the solution was systematically varied. Initially, the pH levels of 3, 5, 7, 9, and 12 were established for BPA. This was achieved by adding 0.1 M HCl and NaOH drop by drop as needed. The degradation trials were conducted under identical conditions with exposure to

sunlight. The degradation efficiency of BPA is highest at pH 7, within a time period of 120 minutes. Fig. S4 illustrates the impact of pH on the breakdown of BPA by $\{[Ca(Cei)(H_2O)_2].3H_2O\}_n$ **(Ca-MOF)** under visible sunlight irradiation for a duration of 120 minutes. The pH levels tested were 3, 5, 7, 9, and 12.

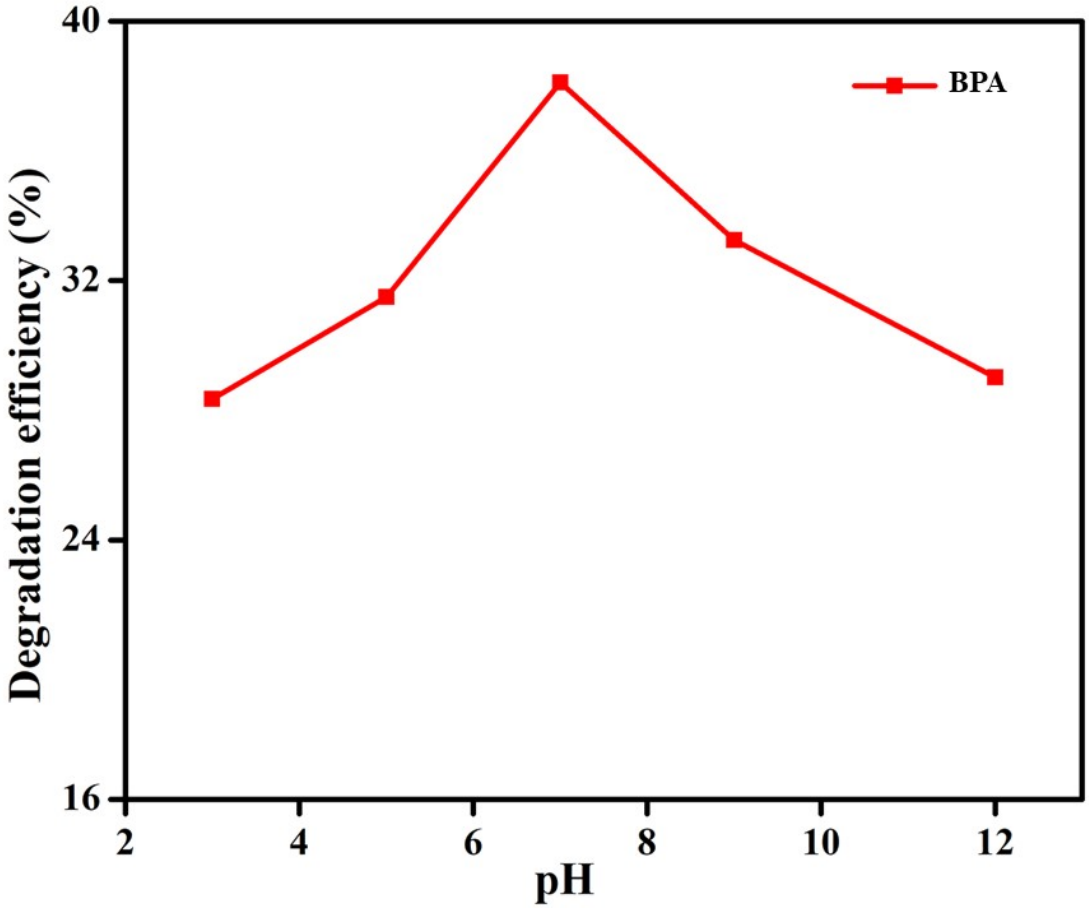

Fig. S4. Investigating the Impact of pH on BPA Degradation with $\{[Ca(Cei)(H_2O)_2].3H_2O\}_n$ **(Ca-MOF)**.

5.4 Capture Study

A study utilizing a UV-Vis spectrophotometer investigated the removal of BPA from polluted water samples. According to the UV-Vis data, $\{[Ca(Cei)(H_2O)_2].3H_2O\}_n$ **(Ca-MOF)** swiftly eliminated BPA with the concentration 6.073 ppm . Within 120 minutes, 37.52% of these BPA

was effectively removed across concentrations 6.073 ppm as demonstrated in Fig. S5 with a contact time of 120 minutes.

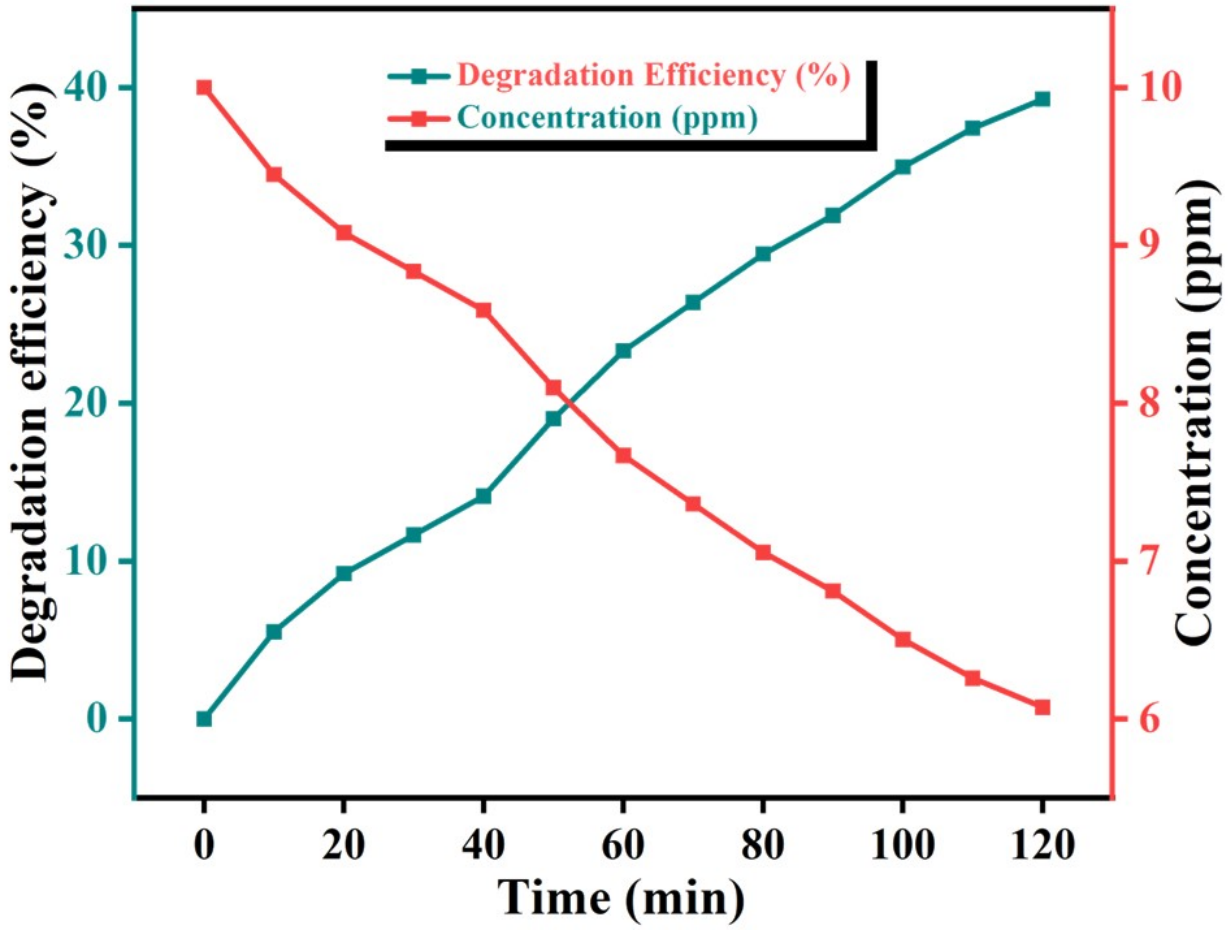

Fig. S5. The adsorption efficiency/concentration of **Ca-MOF** with BPA as a function of contact time (120 minutes).

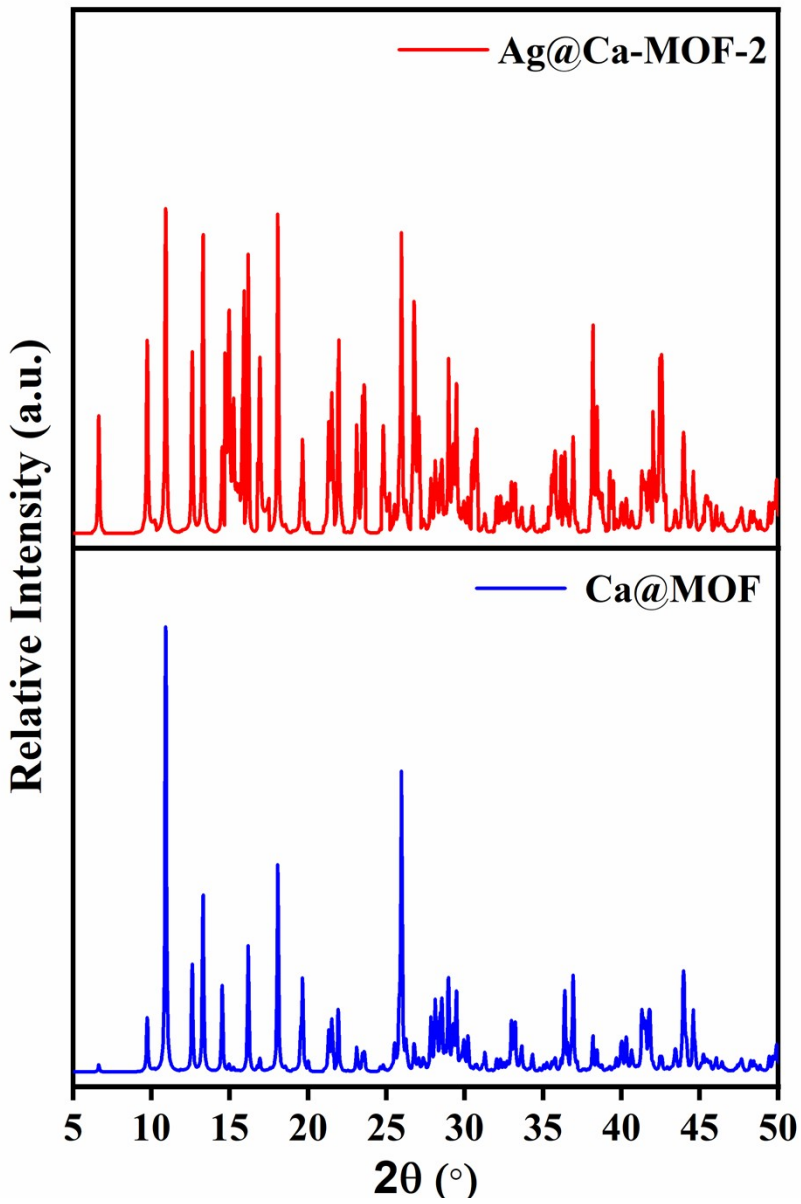

Fig. S6 PXRD spectra of as-synthesized $\{[Ca(Cei)(H_2O)_2].3H_2O\}_n$ Ca-MOF and its silver doped Ag@Ca-MOF-2 composite.

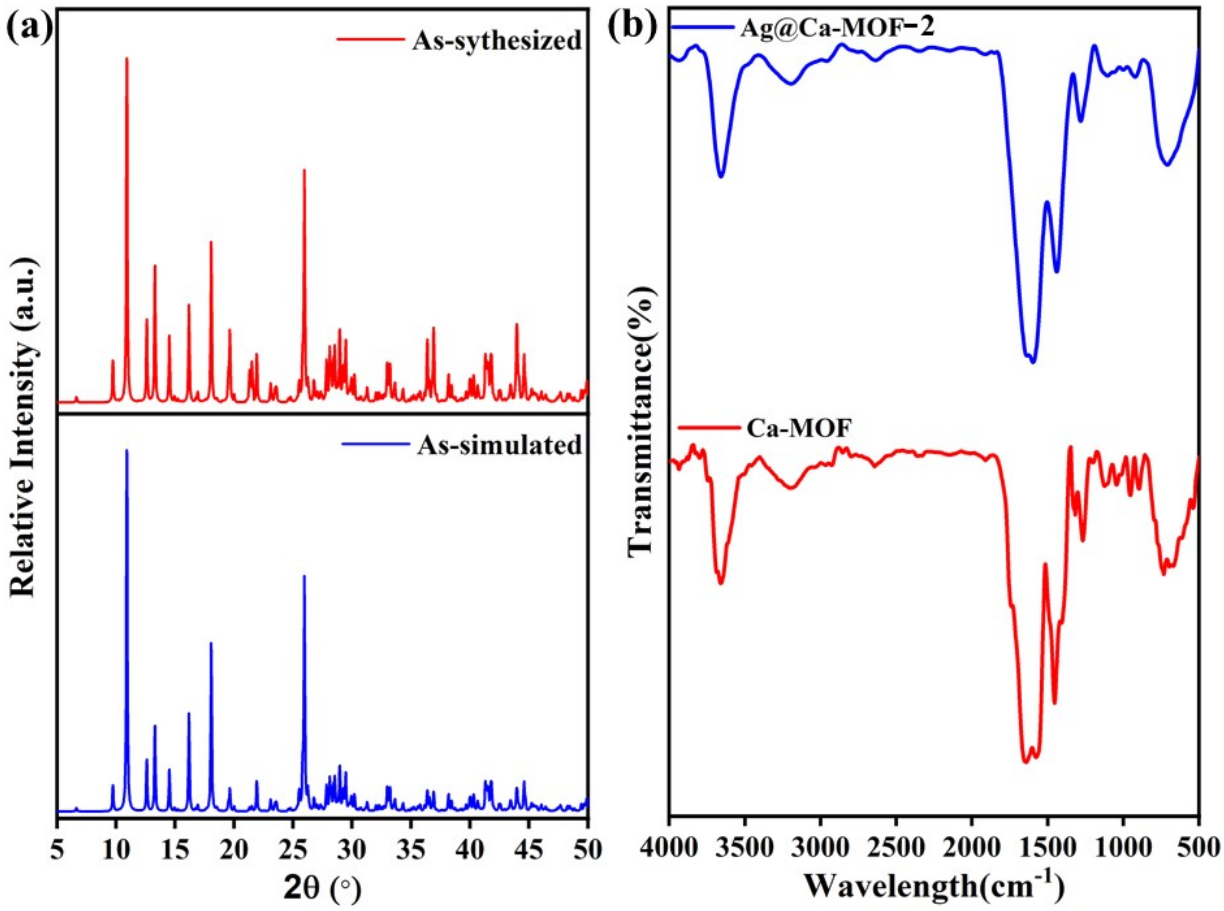

Fig. S7 (a) PXRD patterns displaying the contrast between the simulated and synthesized Ca-MOF crystal; (b) FT-IR spectra highlighting the distinctive features of the synthesized Ca-MOF crystal and the Ag@Ca-MOF-2 composite.

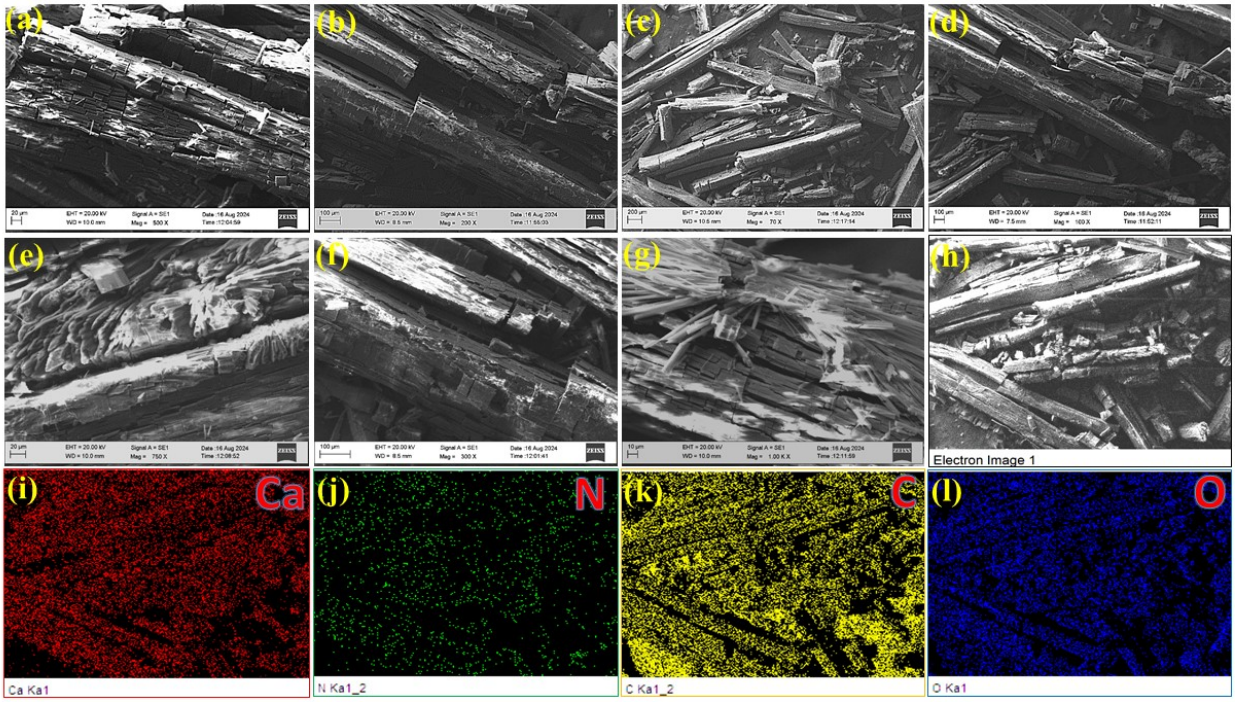

Fig. S8 SEM images of (a-h) Ca-MOF crystals at different magnification and (i-l) electronic image and elemental mapping image of Ca, N, C and O elements.

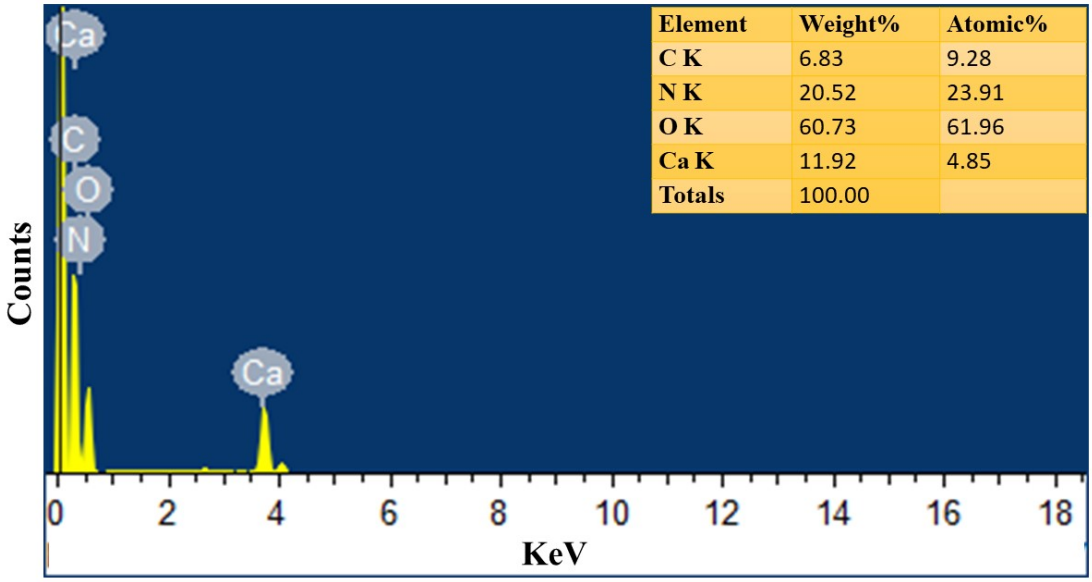

Element	Weight%	Atomic%
C K	6.83	9.28
N K	20.52	23.91
O K	60.73	61.96
Ca K	11.92	4.85
Totals	100.00	

Fig. S9 EDAX analysis of Ca-MOF.

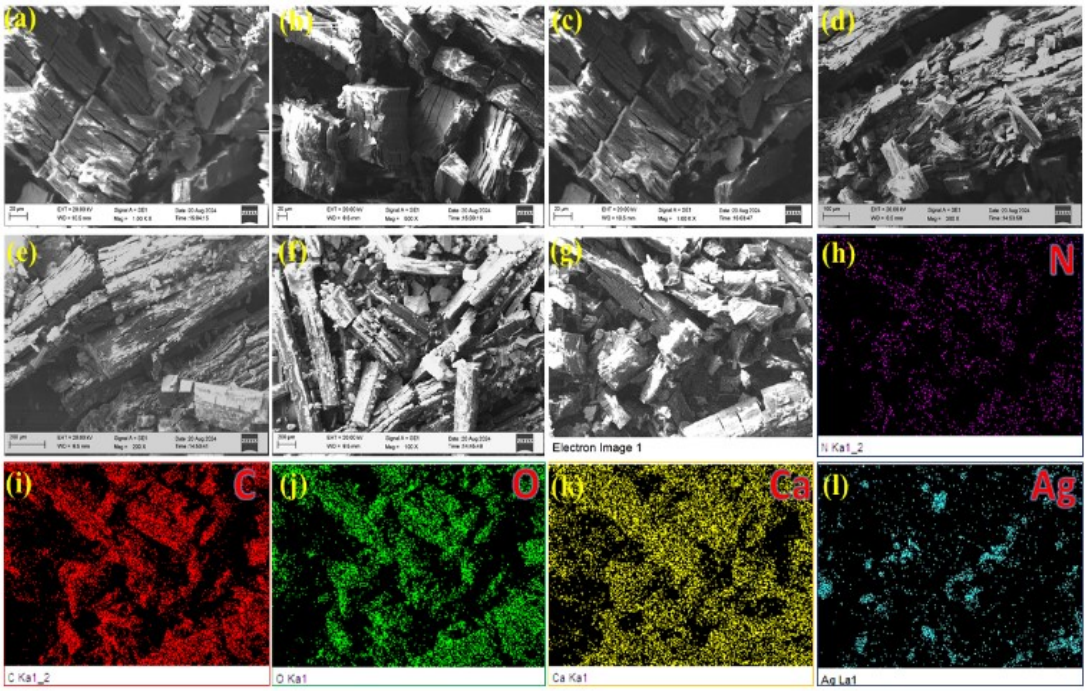

Fig. S10 SEM images depicting the Ag@Ca-MOF-2 composite across various magnifications (a-g) reveal intricate structural details, while images (h-l) showcase the electronic and elemental mapping, illustrating the distribution of nitrogen (N), carbon (C), oxygen (O), calcium (Ca), and silver (Ag) elements within the composite.

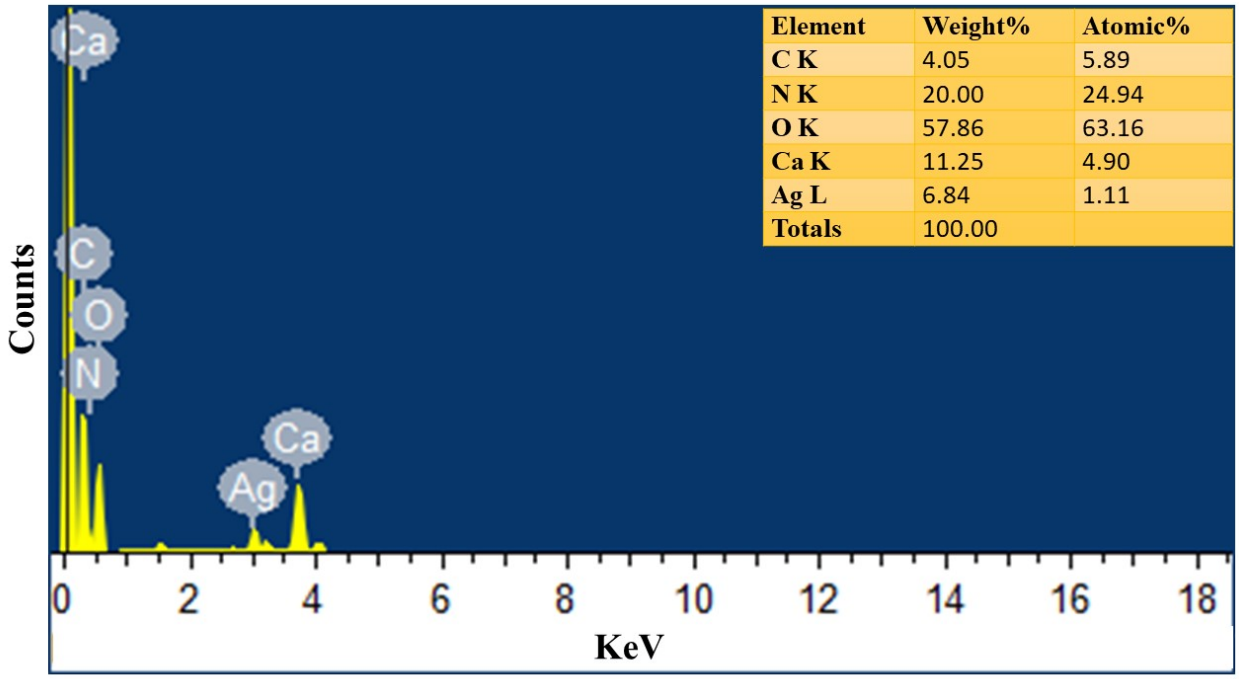

Fig. S11 EDAX analysis of Silver doped Ca-MOF composite (Ag@Ca-MOF).

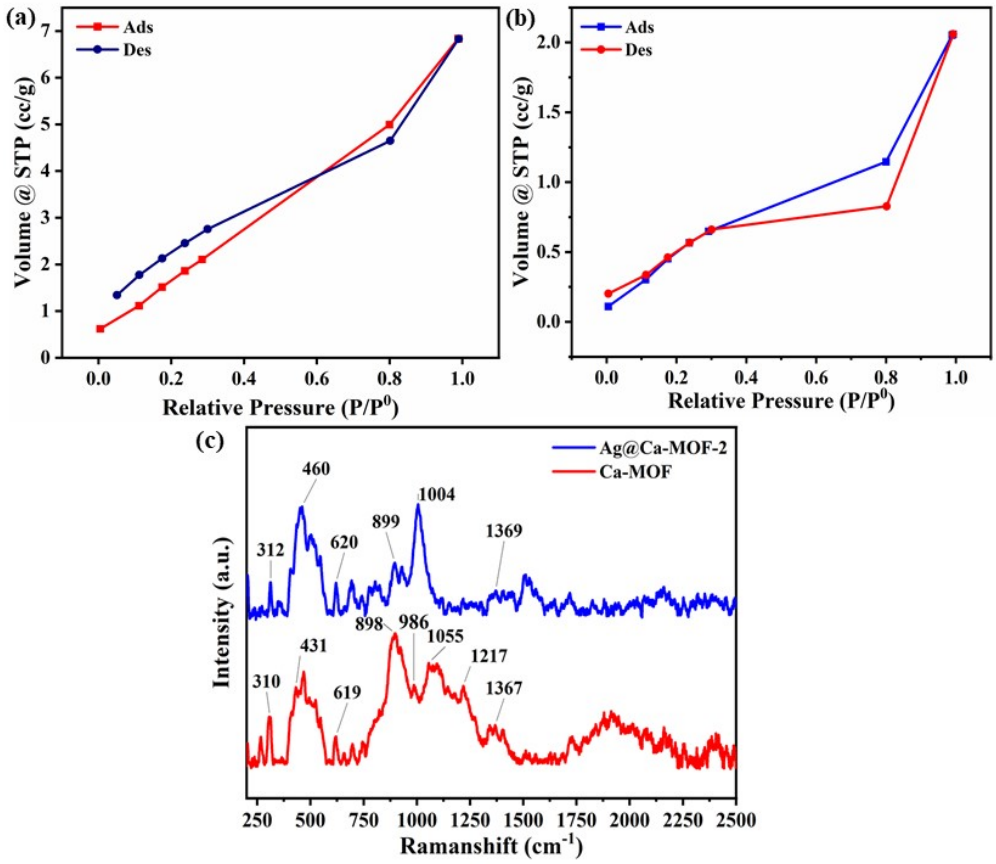

Fig. S12 N2 adsorption−desorption isotherms for the (a) Ca-MOF and (b) Ag@Ca-MOF-2 and (c) Raman spectra of pure crystal (Ca-MOF) and Ag doped Ca-MOF composite (Ag@Ca-MOF-2).

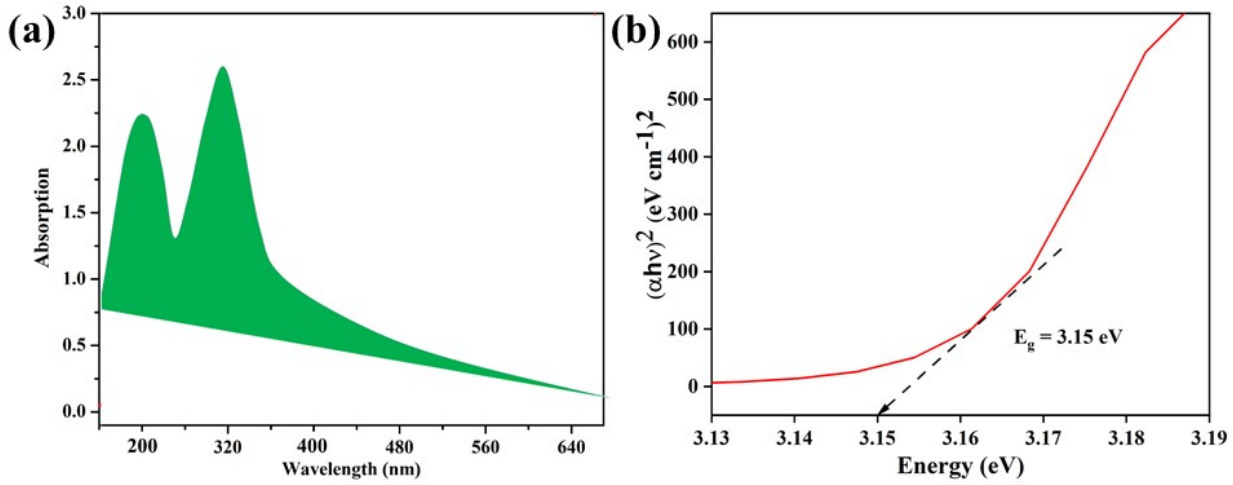

Fig. S13 (a) UV-vis absorption spectra of $\{[Ca(Cei)(H_2O)_2].3H_2O\}_n$ (Ca-MOF) and (b) Tauc plot ($(\alpha h\nu)^2$ vs energy (eV)) for band gap study of $\{[Ca(Cei)(H_2O)_2].3H_2O\}_n$ (Ca-MOF).

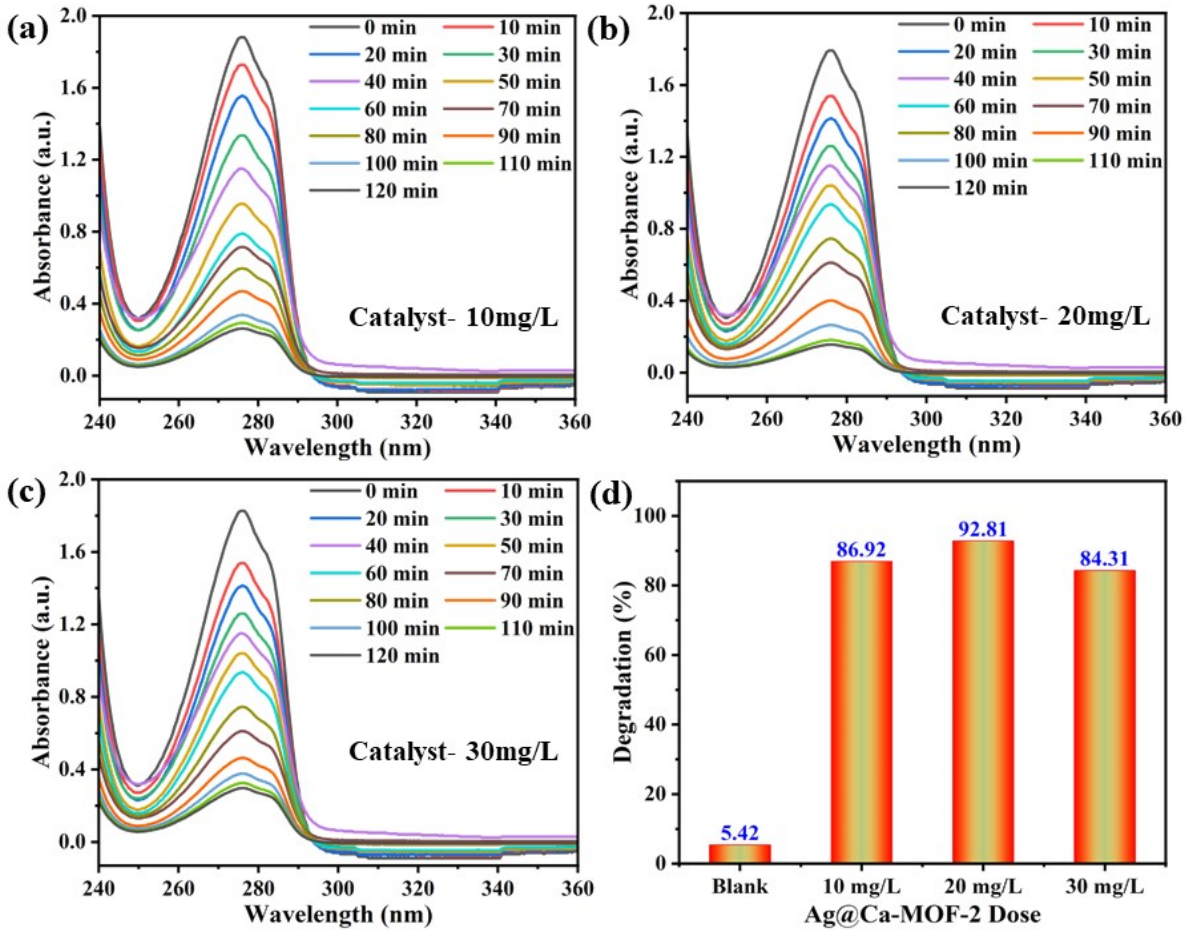

Fig. S14 Photo degradation UV-Vis spectra of BPA with (a) 10 mg/L dose of Ag@Ca-MOF-2, (b) 20 mg/L dose of Ag@Ca-MOF-2, (c) 30 mg/L dose of Ag@Ca-MOF-2 and (d) bar plot indicating the effect of dosages of Ag@Ca-MOF-2 on BPA degradation.

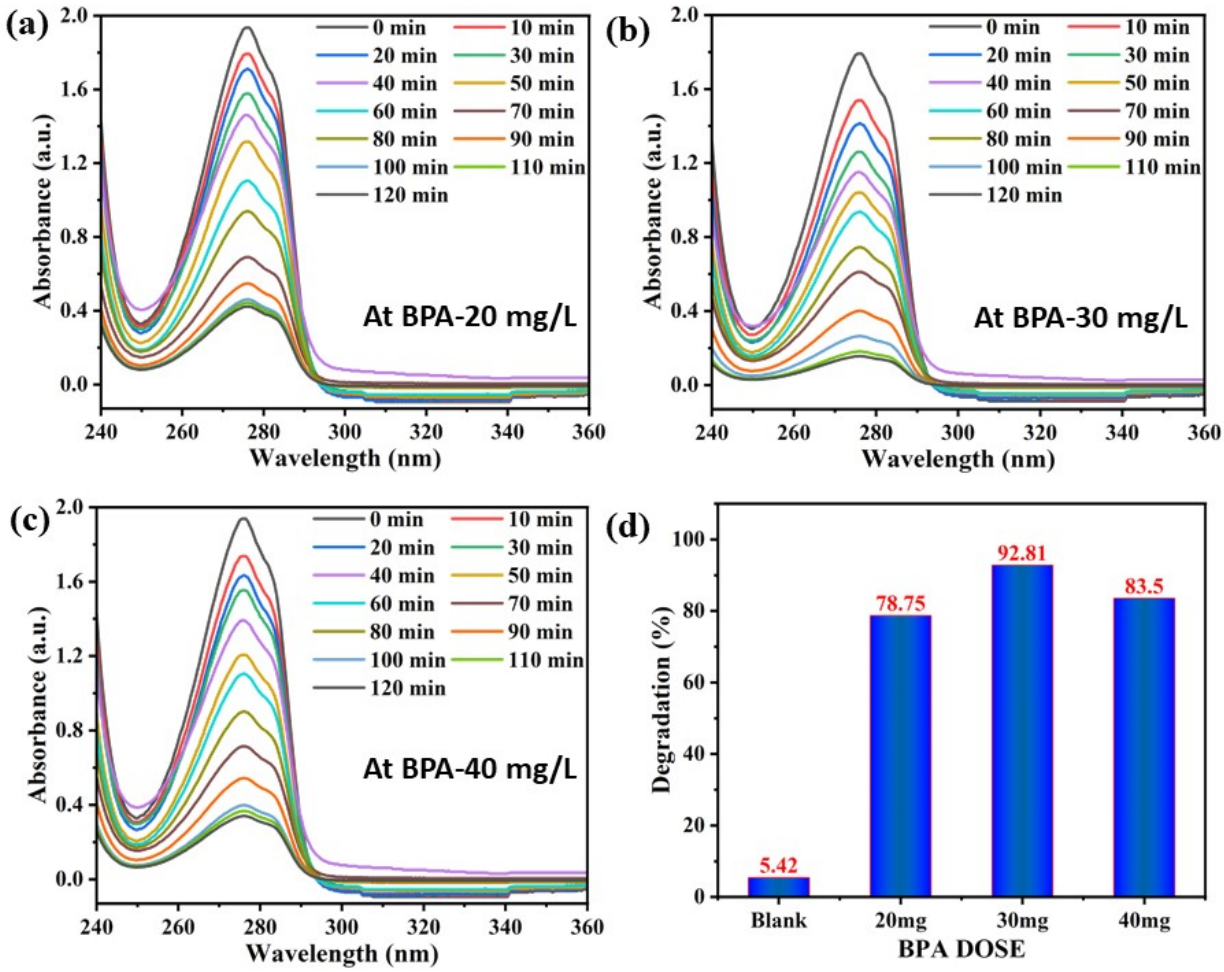

Fig. S15 Photo degradation UV-Vis spectra of BPA with (a) 20 mg/L conc. of BPA, (b) 30 mg/L conc. of BPA, (c) 40 mg/L conc. of BPA, and (d) bar plot indicating the effect of dosages of BPA on degradation efficiency with blank BPA degradation percentage.

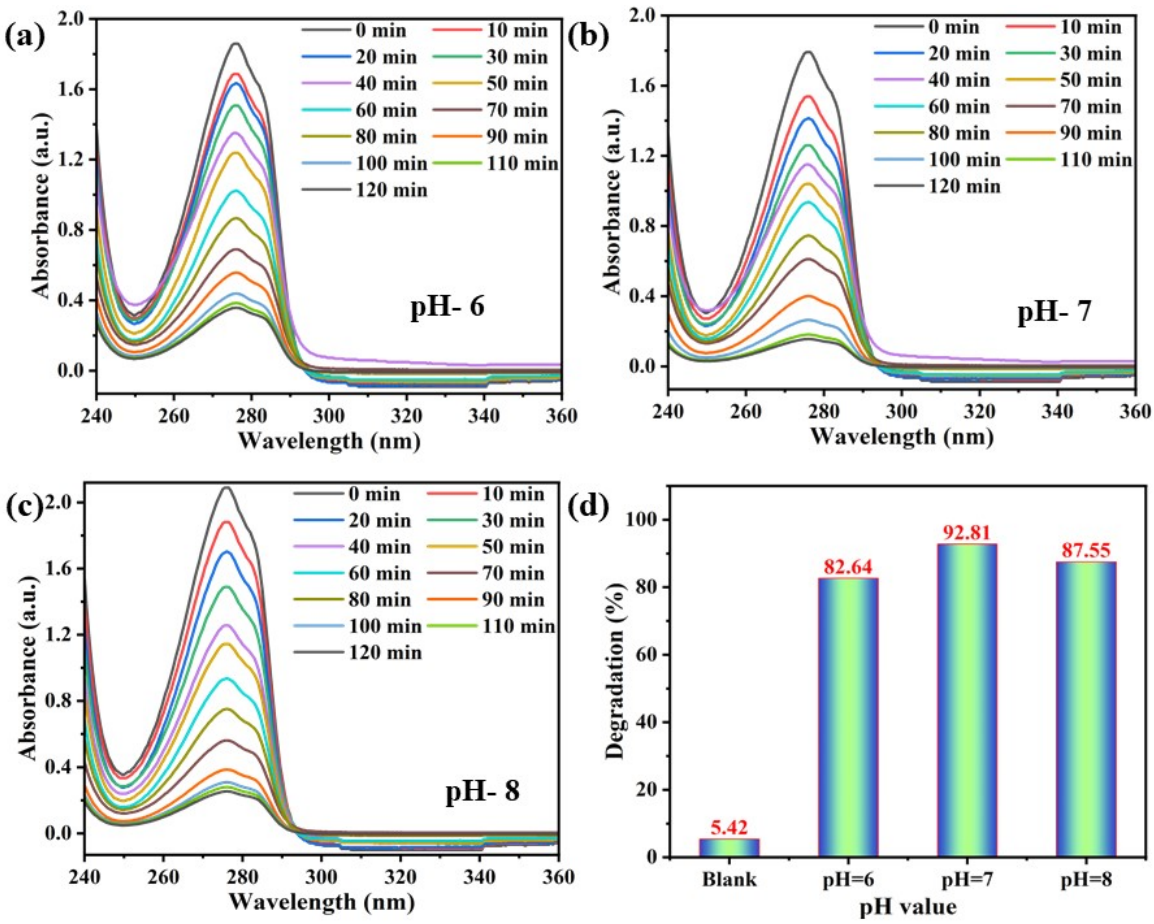

Fig. S16 Photo degradation UV-Vis spectra of BPA with Ag@Ca-MOF-2 at (a) pH – 6, (b) pH – 7, (c) pH – 8, in 120 min. contact time, and (d) bar plot indicating the effect of pH of BPA solution on degradation efficiency with blank BPA degradation percentage.

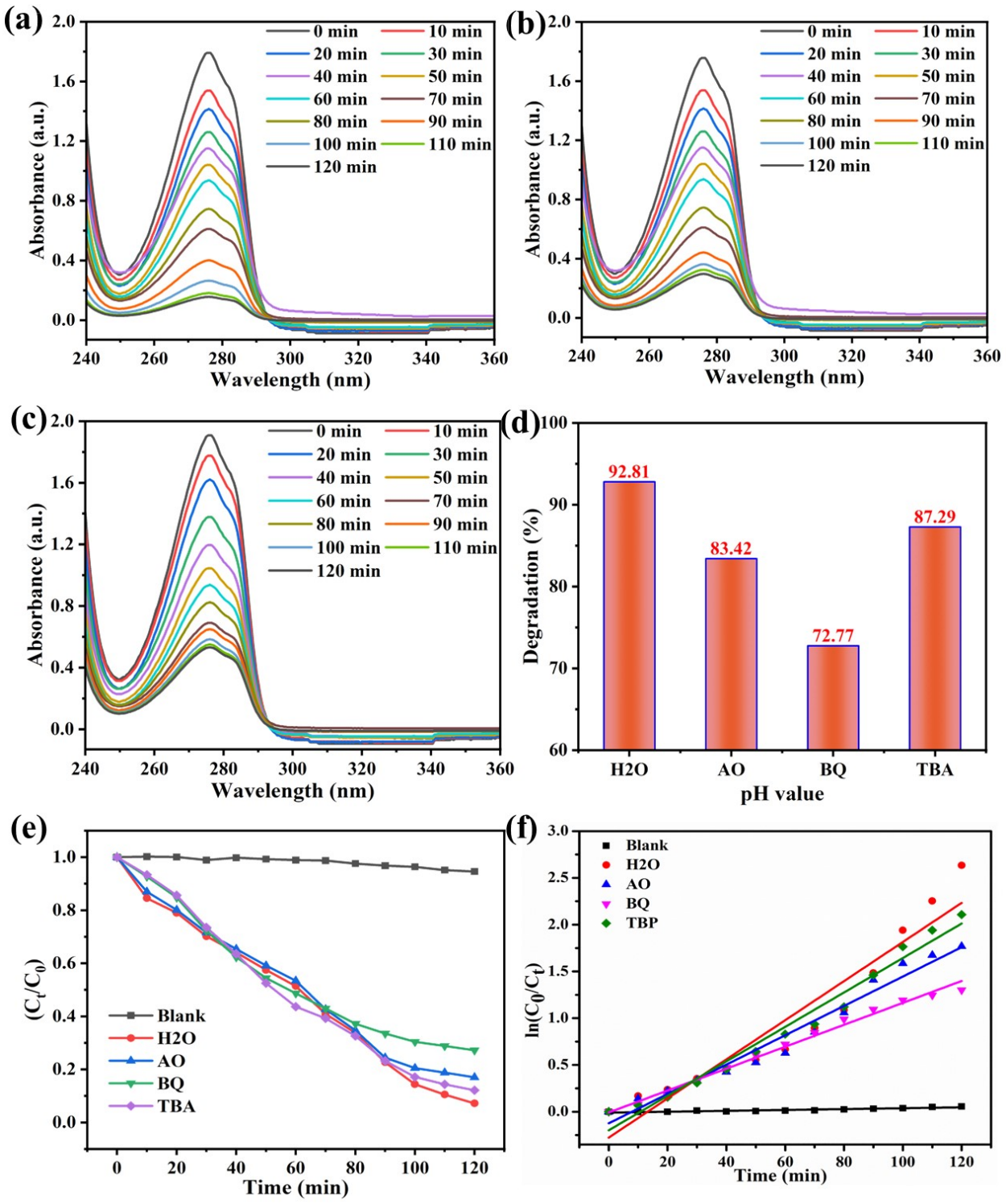

Fig. S17 Photocatalytic UV-Vis spectra showing BPA degradation in the presence of Ag@Ca-MOF-2 along with different scavengers: (a) ammonium oxalate (AO), (b) benzoquinone (BQ), and (c) tertiary

butyl alcohol (TBA). (d) A bar chart demonstrating the impact of various radical trapping agents on BPA photodegradation efficiency. (e) C_t/C_0 vs. irradiation time plot depicting BPA degradation under Ag@Ca-MOF-2 with different trapping agents. (f) Pseudo-first-order kinetics plot illustrating BPA degradation in the presence of Ag@Ca-MOF-2 and the respective trapping agents. Experimental conditions were fixed with 20 mg/L of catalyst, 30 mg/L BPA, and pH 7.

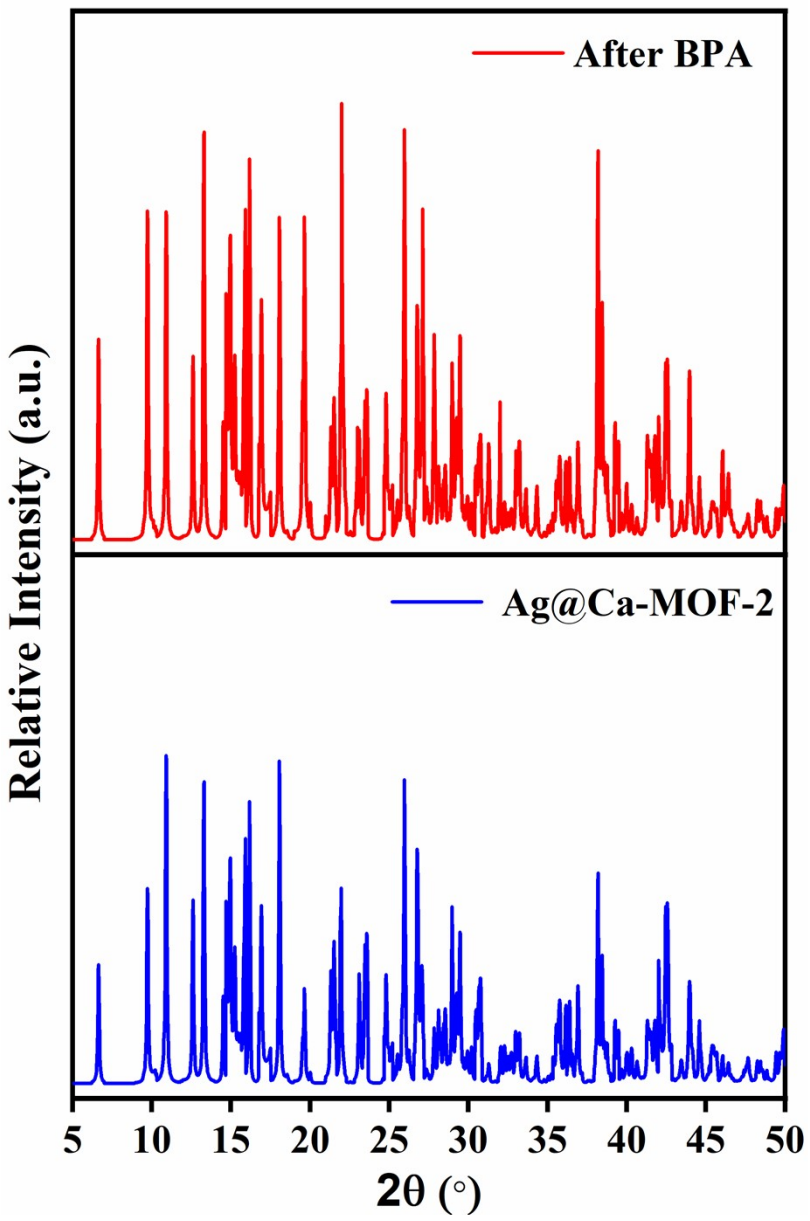

Fig. S18 PXRD spectra of fresh Ag@Ca-MOF-2 and after BPA degradation.

S 2. Photoluminescence Sensing of BPA

S 2.1 Detection of Solvent

An investigation into Bisphenol A (BPA) detection was performed using the synthesized Ca-MOF and its Ag-doped variant, Ag@Ca-MOF-2. For each analysis, a 3 mg sample of the MOF was immersed in 4 mL of various solvents, including water, acetonitrile (CH_3CN), Dichloromethane (DCM), Methanol (MeOH), Acetone, Ethyl alcohol, Diethylformamide (DEF), isopropyl alcohol (IPA), tetrahydrofuran (THF), and dimethylformamide (DMF), Chloroform ($CHCl_3$) and Nitrobenzene (NB) to assess its fluorescence behavior. Each suspension was subjected to ultrasonic treatment for 30 minutes, ensuring homogeneity, and subsequently allowed to settle for 24 hours. Under excitation at 300 nm, the fluorescence of the MOF suspensions was measured across the 200–600 nm range. Water emerged as the solvent with the highest emission intensity and lowest quenching efficiency for both Ca-MOF and Ag@Ca-MOF-2, indicating it as the optimal medium for BPA detection (Fig. S19). This setup allowed for a stable luminescence signal, enabling reliable and reproducible quenching analysis specific to BPA in aqueous media.

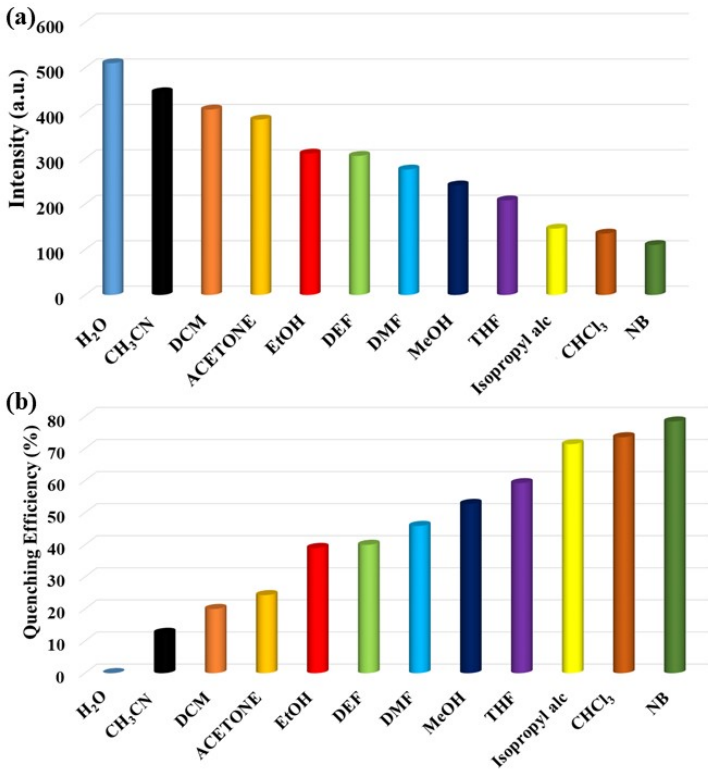

Fig. S19 (a) Fluorescence intensity assessment; (b) Ag@Ca-MOF-2 fluorescence quenching effectiveness in aqueous solutions with different solvents.

S 2.2 The Possible Mechanism of Fluorescence Quenching

Previous studies indicate that identifying components in complex solutions is frequently impacted by framework collapse, ion exchange, and competitive adsorption or interactions, all of which are associated with quenching effects.[26] To gain a deeper understanding of the quenching mechanism induced by Bisphenol A (BPA) on Ag@Ca-MOF-2, we performed UV-vis spectroscopy. The observed quenching of Ag@Ca-MOF-2 in the presence of BPA is not attributed to structural degradation, which suggests that the integrity of the Ag@Ca-MOF-2 framework remains preserved during the sensing process.

The reduction in fluorescence intensity during the electron-transfer transitions involving BPA can be explained by the decreased energy transfer between the π and π* orbitals in the nitrogen-containing ligands.[31] Resonance energy transfer, in this case, depends on the extent of spectral overlap between the excitation band of Ag@Ca-MOF-2 and the UV-vis absorption band of BPA. As shown in Fig. 20c, there is a significant overlap between the excitation spectrum of Ag@Ca-MOF-2 and the absorption spectrum of BPA, indicating that BPA exhibits a pronounced quenching effect due to this spectral alignment.[47] This competition for excitation wavelength energy absorption between BPA and the MOF structure leads to the observed quenching phenomenon. PXRD spectra of Ca-MOF after detection experiment is shown in Fig. S21a.

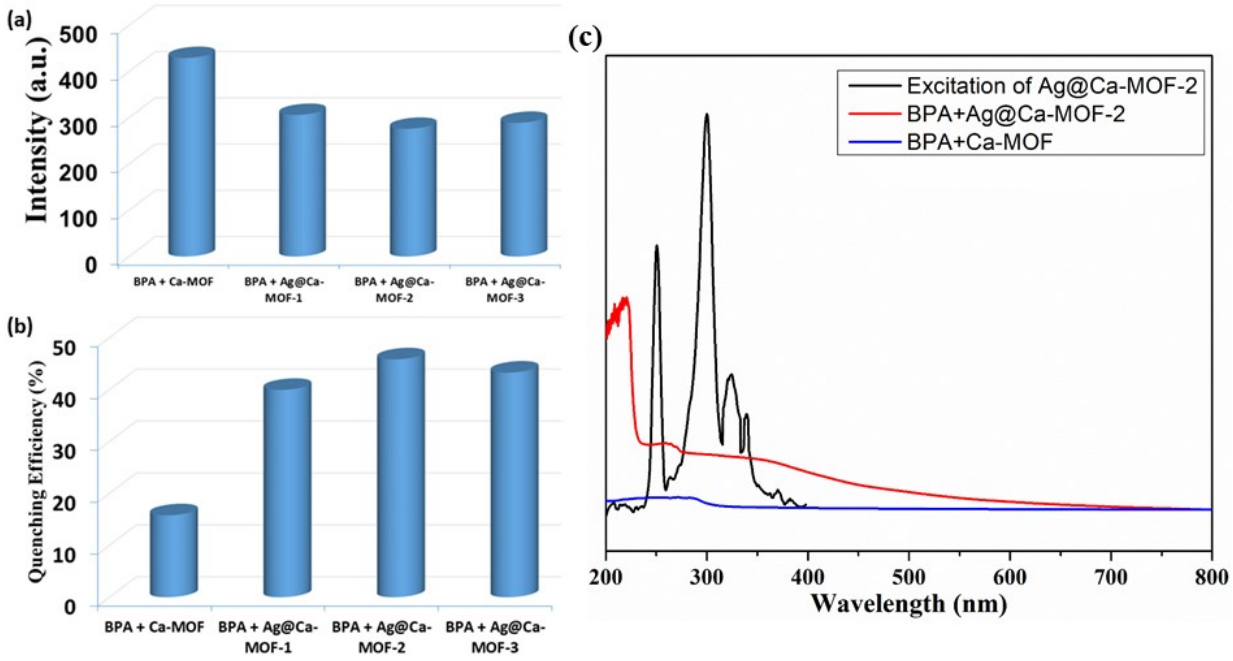

Fig. S20 (a) Intensities and (b) Quenching efficiencies of BPA solution with Ca-MOF and Ag@Ca-MOF composite materials (c) Spectral overlap between the UV-Vis absorption spectra of various analytes and the excitation spectra of Ag@Ca-MOF-2.

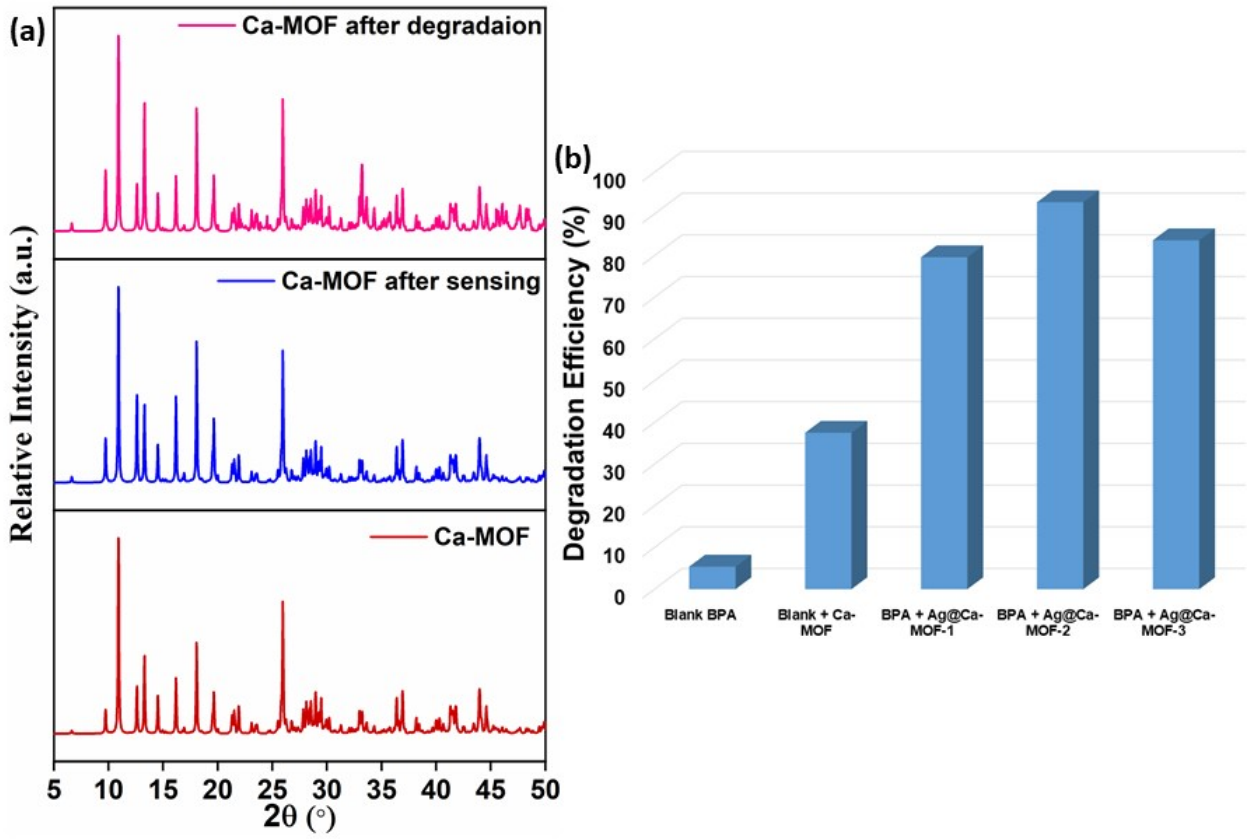

Fig. S21 (a) PXRD spectra of Ca-MOF, after sensing and degradation of BPA, PXRD of Ca-MOF crystal (b) degradation efficiencies of BPA for Blank BPA, BPA+Ca-MOF and Ag doped composites.

Table S1 Extracted data from the XPS analysis for the under-studied samples Ca-MOF.

Sample	Peak	Formula	Peak position (eV)	Peak area (CPS.eV)	Atomic %
Ca-MOF	N 1s	Ca-N	397.80	1115.86	18.53
		C-NH	399.29	3556.98	59.07
		N-H	400.62	1348.42	22.39
	C 1s	C-C/C-H	283.55	5000.56	38.70
		C=C	284.71	2176.00	16.84
		C-O	285.60	1470.54	11.38
		C=O	287.81	4275.36	33.08
	O 1s	Ca-O-C	529.94	3451.19	23.01
		Ca-O	530.73	6799.00	45.33

		O=C-O	531.51	3679.51	24.53
		O-C	532.43	1068.77	7.13
	Ca 2p	Ca metal	345.79	1611.88	17.67
		O-Ca-O	346.66	3692.71	40.49
		O-Ca-N	347.99	988.98	10.84
		Ca metal	349.33	706.97	7.75
		O-Ca-O	350.23	1425.09	15.62
		O-Ca-N	351.37	695.76	7.63

Table S2 Extracted data from the XPS analysis for the under-studied samples Ag@Ca-MOF-2.

Sample	Peak	Formula	Peak position (eV)	Peak area (CPS.eV)	Atomic %
Ag@Ca-MOF-2	N 1s	Ca-N	397.61	380.06	14.48
		C-NH	399.23	1753.74	66.82
		N-H	401.62	490.93	18.70
	C 1s	C-C/C-H	283.39	4064.22	35.17
		C=C	284.09	3179.27	27.51
		C-O	285.09	2313.80	20.02
		C=O	287.78	1999.23	17.30
	O 1s	Ca-O-C	530.06	2186.34	10.79
		Ca-O	531.16	12456.43	61.48
		O=C-O	532.07	3717.01	18.35
		O-C	532.69	1900.11	9.38
	Ca 2p	Ca metal	345.79	1611.88	17.67
		O-Ca-O	346.66	3692.71	40.49
		O-Ca-N	347.99	988.98	10.84
		Ca metal	349.33	706.97	7.75
		O-Ca-O	350.23	1425.09	15.62
		O-Ca-N	351.37	695.76	7.63
	Ag 3d	Ag^0	367.16	23664.20	51.96
		Ag^{2+}	368.10	3307.31	7.26
		Ag^0	373.09	12023.68	26.39
		Ag^{2+}	373.73	6557.76	14.39

Table S3. Lattice parameters refinement data of complex Ca-MOF.

Empirical formula	$C_9H_{19}CaN_3O_{12}$
Formula weight	401.34
Temperature/K	293(2)
Crystal system	monoclinic
Space group	$P2_1/n$
a/Å	21.0666(6)
b/Å	6.85937(16)
c/Å	24.3990(6)
α/°	90
β/°	107.741(3)
γ/°	90
Volume/Å^3	3358.08(16)
Z	8
ρ_{calc}g/cm^3	1.5875
μ/mm^{-1}	3.880
F(000)	1690.1
Crystal size/mm^3	0.45 × 0.23 × 0.16
Radiation	Cu Kα (λ = 1.54184)
2Θ range for data collection/°	4.86 to 136.22
Index ranges	$-25 \le h \le 25$, $-8 \le k \le 7$, $-29 \le l \le 29$
Reflections collected	36339
Independent reflections	6092 [R_{int} = 0.0399, R_{sigma} = 0.0236]
Data/restraints/parameters	6092/2/508
Goodness-of-fit on F^2	1.035
Final R indexes [I>=2σ (I)]	R_1 = 0.0356, wR_2 = 0.1079
Final R indexes [all data]	R_1 = 0.0400, wR_2 = 0.1115
Largest diff. peak/hole / e Å^{-3}	0.40/-0.53
CCDC No.	2391823

Table. S4 Bond Lengths for Ca-MOF.

Atom	Atom	Length/Å		Atom	Atom	Length/Å
Ca1	O10[1]	2.4862(12)		Ca2	O1[4]	2.4770(12)
Ca1	O11[1]	2.5553(12)		Ca2	O2[4]	2.5840(12)
Ca1	O15[2]	2.4482(10)		Ca2	O6[5]	2.7089(11)
Ca1	O15[3]	2.3806(12)		Ca2	O6[6]	2.3837(12)
Ca1	O16	2.3427(11)		Ca2	O7	2.3580(12)
Ca1	O16[2]	2.7690(11)		Ca2	O7[5]	2.4678(10)
Ca1	O17	2.4029(12)		Ca2	O8	2.4034(13)

Ca1	O18	2.3988(14)		Ca2	O9	2.3920(12)
Ca1	C10[1]	2.8610(16)		Ca2	C1[4]	2.8683(16)
Ca1	C18[2]	2.9624(16)		Ca2	C9[5]	2.9426(15)
O10	C10	1.258(2)		O1	C1	1.257(2)
O11	C10	1.246(2)		O2	C1	1.242(2)
O12	C13	1.2122(19)		O3	C4	1.2116(18)
O13	C14	1.2117(18)		O4	C5	1.2125(19)
O14	C15	1.211(2)		O5	C6	1.211(2)
O15	C18	1.2592(19)		O6	C9	1.2457(19)
O16	C18	1.2453(18)		O7	C9	1.2620(19)
N4	C12	1.4711(19)		N1	C3	1.4718(18)
N4	C13	1.382(2)		N1	C4	1.3830(19)
N4	C15	1.392(2)		N1	C6	1.391(2)
N5	C13	1.364(2)		N2	C4	1.365(2)
N5	C14	1.369(2)		N2	C5	1.372(2)
N6	C14	1.3801(19)		N3	C5	1.3787(19)
N6	C15	1.383(2)		N3	C6	1.383(2)
N6	C16	1.4790(17)		N3	C7	1.4781(18)
C10	C11	1.524(2)		C1	C2	1.523(2)
C11	C12	1.522(2)		C2	C3	1.522(2)
C16	C17	1.508(2)		C7	C8	1.511(2)
C17	C18	1.507(2)		C8	C9	1.506(2)

Symmetry element for Calcium - 11/2-X,1/2+Y,3/2-Z; 2-X,2-Y,1-Z; 3+X,1+Y,+Z; 41-X,1-Y,1-Z; 51/2-X,-1/2+Y,1/2-Z; 6+X,-1+Y,+Z

Table. S5 Bond Angles for Ca-MOF.

Atom	Atom	Atom	Angle/°		Atom	Atom	Atom	Angle/°
O11[1]	Ca1	O10[1]	51.49(4)		O2[6]	Ca2	O1[6]	51.13(4)
O15[2]	Ca1	O10[1]	90.90(4)		O6[7]	Ca2	O1[6]	79.96(4)
O15[3]	Ca1	O10[1]	79.77(4)		O6[5]	Ca2	O1[6]	91.06(4)
O15[3]	Ca1	O11[1]	121.74(4)		O6[5]	Ca2	O2[6]	83.39(4)
O15[2]	Ca1	O11[1]	81.39(4)		O6[7]	Ca2	O2[6]	126.61(4)
O16	Ca1	O10[1]	84.92(4)		O7	Ca2	O1[6]	86.33(4)
O16[3]	Ca1	O10[1]	78.69(4)		O7[7]	Ca2	O1[6]	78.27(4)
O16	Ca1	O11[1]	86.79(4)		O7	Ca2	O2[6]	86.44(4)
O16[3]	Ca1	O11[1]	128.02(4)		O7[7]	Ca2	O2[6]	123.16(4)
O16[3]	Ca1	O15[3]	49.16(4)		O7[7]	Ca2	O6[7]	49.79(3)
O16	Ca1	O15[2]	167.47(4)		O7	Ca2	O6[7]	68.34(3)
O16[3]	Ca1	O15[2]	117.24(3)		O7[7]	Ca2	O6[5]	72.24(4)
O16	Ca1	O15[3]	122.45(4)		O7	Ca2	O6[5]	168.72(4)

O17	Ca1	O10[1]	131.92(5)		O8	Ca2	O1[6]	130.01(5)
O17	Ca1	O11[1]	80.60(4)		O8	Ca2	O2[6]	79.24(5)
O17	Ca1	O15[2]	84.87(4)		O8	Ca2	O6[5]	88.45(5)
O17	Ca1	O15[3]	139.63(5)		O8	Ca2	O6[7]	139.21(5)
O17	Ca1	O16[3]	144.07(4)		O8	Ca2	O7	84.85(4)
O17	Ca1	O16	89.15(4)		O8	Ca2	O7[7]	146.89(4)
O18	Ca1	O10[1]	146.79(5)		O9	Ca2	O1[6]	152.20(5)
O18	Ca1	O11[1]	155.40(5)		O9	Ca2	O2[6]	153.88(5)
O18	Ca1	O15[2]	108.37(5)		O9	Ca2	O6[5]	84.44(5)
O18	Ca1	O15[3]	82.72(5)		O9	Ca2	O6[7]	79.31(5)
O18	Ca1	O16[3]	68.53(5)		O9	Ca2	O7	102.88(5)
O18	Ca1	O16	81.00(5)		O9	Ca2	O7[7]	74.22(4)
O18	Ca1	O17	77.95(5)		O9	Ca2	O8	77.41(5)
C10[1]	Ca1	O10[1]	26.02(4)		C1[6]	Ca2	O1[6]	25.90(4)
C10[1]	Ca1	O11[1]	25.81(4)		C1[6]	Ca2	O2[6]	25.66(4)
C10[1]	Ca1	O15[2]	82.67(4)		C1[6]	Ca2	O6[7]	104.98(4)
C10[1]	Ca1	O15[3]	99.48(4)		C1[6]	Ca2	O6[5]	83.50(4)
C10[1]	Ca1	O16[3]	104.41(4)		C1[6]	Ca2	O7	89.45(4)
C10[1]	Ca1	O16	88.50(4)		C1[6]	Ca2	O7[7]	99.46(4)
C10[1]	Ca1	O17	106.38(5)		C1[6]	Ca2	O8	104.89(5)
C10[1]	Ca1	O18	168.64(6)		C1[6]	Ca2	O9	167.65(5)
C18[3]	Ca1	O10[1]	80.90(4)		C9[7]	Ca2	O1[6]	80.81(4)
C18[3]	Ca1	O11[1]	131.62(4)		C9[7]	Ca2	O2[6]	131.88(4)
C18[3]	Ca1	O15[2]	92.63(4)		C9[7]	Ca2	O6[7]	25.03(4)
C18[3]	Ca1	O15[3]	24.64(4)		C9[7]	Ca2	O6[5]	97.05(4)
C18[3]	Ca1	O16[3]	24.80(4)		C9[7]	Ca2	O7	93.37(4)
C18[3]	Ca1	O16	98.35(4)		C9[7]	Ca2	O7[7]	25.06(4)
C18[3]	Ca1	O17	147.03(5)		C9[7]	Ca2	O8	148.75(5)
C18[3]	Ca1	O18	71.67(5)		C9[7]	Ca2	O9	72.59(5)
C18[3]	Ca1	C10[1]	105.88(5)		C9[7]	Ca2	C1[6]	106.29(5)
C10	O10	Ca1[4]	93.87(10)		C1	O1	Ca2[6]	94.71(10)
C10	O11	Ca1[4]	90.93(9)		C1	O2	Ca2[6]	90.07(10)
C18	O15	Ca1[5]	146.44(10)		C9	O6	Ca2[2]	165.38(10)
C18	O15	Ca1[3]	101.19(9)		C9	O6	Ca2[8]	88.04(9)
C18	O16	Ca1[3]	86.32(9)		C9	O7	Ca2	143.73(10)
C18	O16	Ca1	167.20(10)		C9	O7	Ca2[8]	99.02(9)
C13	N4	C12	118.19(13)		C4	N1	C3	118.21(12)
C15	N4	C12	118.16(13)		C6	N1	C3	118.00(12)
C15	N4	C13	123.63(13)		C6	N1	C4	123.70(13)
C14	N5	C13	125.97(13)		C5	N2	C4	125.91(13)
C15	N6	C14	123.73(13)		C6	N3	C5	123.72(13)
C16	N6	C14	118.03(12)		C7	N3	C5	118.27(12)
C16	N6	C15	118.15(12)		C7	N3	C6	117.97(12)
O10	C10	Ca1[4]	60.11(8)		O1	C1	Ca2[6]	59.39(8)
O11	C10	Ca1[4]	63.26(8)		O2	C1	Ca2[6]	64.27(9)

O11	C10	O10	122.06(15)		O2	C1	O1	122.01(15)
C11	C10	Ca1[4]	168.70(12)		C2	C1	Ca2[6]	166.76(11)
C11	C10	O10	119.14(15)		C2	C1	O1	118.79(15)
C11	C10	O11	118.80(15)		C2	C1	O2	119.20(15)
C12	C11	C10	109.77(14)		C3	C2	C1	110.29(14)
C11	C12	N4	110.55(14)		C2	C3	N1	110.27(14)
N4	C13	O12	122.46(15)		N1	C4	O3	122.61(14)
N5	C13	O12	122.27(15)		N2	C4	O3	122.20(14)
N5	C13	N4	115.27(14)		N2	C4	N1	115.18(13)
N5	C14	O13	121.60(14)		N2	C5	O4	121.39(14)
N6	C14	O13	123.02(14)		N3	C5	O4	123.19(14)
N6	C14	N5	115.36(13)		N3	C5	N2	115.40(13)
N4	C15	O14	121.69(15)		N1	C6	O5	121.62(15)
N6	C15	O14	122.32(15)		N3	C6	O5	122.31(15)
N6	C15	N4	116.00(13)		N3	C6	N1	116.07(14)
C17	C16	N6	109.85(13)		C8	C7	N3	110.34(13)
C18	C17	C16	115.05(14)		C9	C8	C7	114.70(14)
O15	C18	Ca1[3]	54.17(7)		O6	C9	Ca2[8]	66.94(8)
O16	C18	Ca1[3]	68.88(8)		O7	C9	Ca2[8]	55.92(7)
O16	C18	O15	121.92(14)		O7	C9	O6	121.71(14)
C17	C18	Ca1[3]	165.22(11)		C8	C9	Ca2[8]	166.03(11)
C17	C18	O15	116.60(13)		C8	C9	O6	121.67(14)
C17	C18	O16	121.48(14)		C8	C9	O7	116.62(14)

Symmetry element for Calcium - 1/2-X,1/2+Y,3/2-Z; 2+X,1+Y,+Z; 3-X,2-Y,1-Z; 41/2-X,-1/2+Y,3/2-Z; 5+X,-1+Y,+Z; 61-X,1-Y,1-Z; 71/2-X,-1/2+Y,1/2-Z; 81/2-X,1/2+Y,1/2-Z

Table S6 H- Bonding interaction and bond distance for Ca-MOF.

Atom	Atom	Distance/Å		Atom	Atom	Length/Å
O5	H21[b]	2.129		O19	H24[b]	1.900
O2	H21[a]	1.915		O14	H19[a]	1.919
O21	H5	1.870		O23	H22[a]	1.960
O14	H20[b]	2.139		O13	H23[b]	1.953
O11	H20[a]	1.923		O22	H22[b]	1.775
O20	H2	1.877		O24	H24[a]	1.776